Influence of confinement on dynamical heterogeneities in dense colloidal samples

Kazem V. Edmond,* Carolyn R. Nugent,† and Eric R. Weeks
Physics Department, Emory University, Atlanta, Georgia 30322, USA
(Received 30 January 2012; published 11 April 2012)

We study a dense colloidal suspension confined between two quasiparallel glass plates as a model system for a supercooled liquid in confined geometries. We directly observe the three-dimensional Brownian motion of the colloidal particles using laser scanning confocal microscopy. The particles form dense layers along the walls, but crystallization is avoided as we use a mixture of two particle sizes. A normally liquidlike sample, when confined, exhibits slower diffusive motion. Particle rearrangements are spatially heterogeneous, and the shapes of the rearranging regions are strongly influenced by the layering. These rearranging regions become more planar upon confinement. The wall-induced layers and changing character of the spatially heterogeneous dynamics appear strongly connected to the confinement-induced glassiness.

DOI: 10.1103/PhysRevE.85.041401 PACS number(s): 82.70.Dd, 64.70.pv, 61.43.Fs

I. INTRODUCTION

As a glass-forming liquid is cooled, its viscosity increases smoothly but dramatically by many orders of magnitude. The macroscopic divergence in viscosity is related to the divergence in the microscopic structural relaxation time, or α-relaxation time. A conceptual explanation is the Adams and Gibbs hypothesis, which states that the flow in a supercooled liquid involves the cooperative motion of molecules and that the structural arrest at the glass transition is due to a divergence of the size of these cooperatively rearranging regions (CRRs) [1].

Computer simulations and experiments have explored the sizes and shapes of regions of cooperatively moving molecules as a liquid's glass transition is approached [2,3]. A direct means of probing the dynamic length scales of glass-forming liquids is by confining them to smaller volumes, such as within thin films and nanopores. Confinement can either increase, decrease, or even maintain a material's glass transition temperature T_G [4,5]. Both simulation and experiment suggest that the effect on T_G depends on the nature of the interaction between the sample and its confining boundary [6–12]. Attractive interactions may result in an increase in T_G whereas repulsive interactions may result in a decrease [10,13]. Frustration of structural ordering, via a rough surface, for example, can also play a key role, although this can either cause slower or faster dynamics [7,11,14]. Whether or not the restriction of the length scales accessible to CRRs is responsible for the variation in T_G remains to be seen due to the inability to directly observe molecular interactions within glass-forming liquids.

Instead of studying molecular glass formers, we use dense colloidal suspensions of sterically stabilized micrometer-sized spherical particles. Colloidal suspensions have often been used as experimental models of a hard sphere glass [15,16]. We confine our samples within a planar volume formed by two quasiparallel solid surfaces [17], similar to confined colloids studied by other groups [11,18,19]. We use high-speed confocal microscopy to rapidly visualize and acquire three-dimensional images of the particle positions [20–23]. Subsequent image analysis lets us track the individual particle trajectories, providing an accurate picture of the cooperatively rearranging groups of particles. Near the colloidal glass transition ($\phi_g \approx 0.58$ [15]), particles rearrange in groups characterized by a length scale of ~3–6 particle diameters [22,24].

In this paper we further investigate our results from prior experiments that studied confined samples, as pictured in Fig. 1 [17]. Here we focus specifically on the nature of cooperative rearrangements within the confined sample and how they relate to the system's increased glassiness. In these experiments we found that confinement induces glassy behavior at concentrations in which the bulk behavior is still liquidlike. Here, we examine rearranging groups of particles defined by (1) particles making large displacements at some moment in time that are also (2) nearest neighbors with at least one other particle within the group. We show that confining colloidal liquids within a planar volume results in cooperatively rearranging groups of particles that are similarly planar shaped. The flattening shapes of the cooperatively rearranging groups are correlated with the overall slowing of the dynamics, suggesting a connection between confinement, wall-induced structure, and glassy behavior.

Understanding the effects of confinement on the glass transition may help us understand the glass transition in the bulk. Perhaps more importantly, understanding the properties of confined fluids also has direct relevance with lubrication [25], the flow of liquids through microfluidic devices [26,27], and the kinetics of protein folding [28].

II. EXPERIMENTAL DETAILS

A. Colloidal samples and microscopy

We use spherical colloidal poly-methyl-methacrylate (PMMA) particles that are sterically stabilized to prevent interparticle attraction [15,23]. The particles are suspended in a mixture of solvents, cyclohexyl bromide and decalin, to match both their density and index of refraction [23]. While our sample is similar to other types of colloidal suspensions that act like hard spheres [15], the

*Present address: Center for Soft Matter Research, Dept. of Physics, New York University, New York, NY, USA.
†Present address: Department of Earth and Space Sciences, UCLA, Los Angeles, CA, USA.

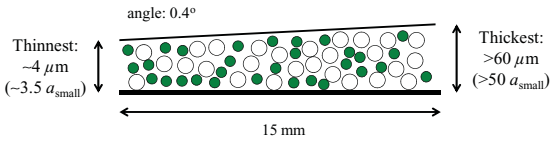

FIG. 1. (Color online) Sketch of sample chamber (not to scale). The small particles are 1.18 μm in radius and are shaded to indicate their fluorescent dye. The large particles are 1.55 μm in radius and drawn in white to indicate their lack of dye, making them invisible to the confocal microscope. One of the boundaries is a coverslip, rather than a glass slide, indicated by the thinner line.

cyclohexylbromide in our solvent mixture induces a slight charge on the surfaces of the particles. Thus, the particles have a slightly soft repulsive interaction in addition to their hard sphere core. To prevent crystallization, which would be readily induced by the smooth walls in our thin planar geometry [29–31], we use a binary mixture of particles with hydrodynamic radii of $a_{\text{small}} = 1.18$ μm and $a_{\text{large}} = 1.55$ μm. The number ratio is approximately $N_S/N_L = 3.5$, and the individual volume fractions are approximately $\phi_S = 0.26, \phi_L = 0.16$, so the total overall volume fraction is $\phi = 0.42 \pm 0.05$. The uncertainty of ϕ arises from the difficulty in precisely determining the individual species' particle size, the polydispersity of particle sizes (~5% for both species), and difficulties in determining the relative volume fractions of the two species [32]. A study of a similar colloidal mixture found the glass transition for bulk samples to be at $\phi_g \approx 0.58$ [33].

We use laser scanning confocal microscopy to view the sample [23]. We can acquire a three-dimensional image of the sample by scanning a $50 \times 50 \times 20$-μm^3 region (equal to $256 \times 256 \times 100$ pixels). We use Visitech's "vt-Eye" confocal system which can scan this volume in 2.0 s. This is much faster than the time for particles to diffuse their own diameter, which is ~100 s in our samples. We acquire sequences of three-dimensional (3D) confocal images every 2.0 s for up to 45 min. By scanning different locations, we observe the behavior at different chamber thicknesses ranging from ~6 μm to ~19 μm in addition to the sample's bulk. Data representing the "bulk" of our sample is acquired from a 20-μm thick subvolume in the thicker region of the sample chamber that is over 15 μm away from the chamber's walls to avoid any boundary effects.

The small particles are dyed with Rhodamine dye [23] and the larger ones are left undyed. Thus the data in our results are for the smaller particles only. Each image is postprocessed to find particle positions with an accuracy of 0.05 μm in x and y (parallel to the walls) and 0.1 μm in z (perpendicular to the walls, and parallel to the optical axis of the microscope). Given that the particles do not move much between images, we can link the particle positions in time to get 3D trajectories of the particles' motion throughout the sample volume [23,34].

B. Sample chambers

Our goal is to study our sample with a range of confinement thicknesses. Here we focus on "thin film" confinement between two flat surfaces. We achieve this by constructing a wedge-shaped sample chamber, as shown in Fig. 1. We build the chamber using a glass slide, a rectangular glass coverslip,

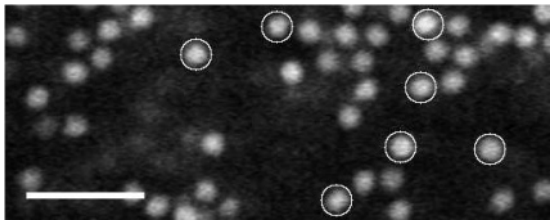

FIG. 2. Typical two-dimensional (2D) confocal microscope image showing particles immediately adjacent to one of the chamber walls. The circled particles are stuck to the glass, and the others move freely. There are also undyed particles also stuck to the surface, as well as undyed mobile particles, which are not visible in this confocal image. The scale bar indicates 10 μm.

and a narrow piece of a ~60-μm-thick Mylar film, employing a method similar to the one used by Refs. [35,36]. Using UV-curing epoxy (Norland 68) we attach the Mylar film near one end of one side of the glass slide so that it runs perpendicular to the slide's length. Next, the glass coverslip is laid across the slide so that one end is raised up by the Mylar film. Meanwhile, the coverslip's opposite end is clamped down, ensuring the thinnest gap size possible. We seal the sample chamber shut with epoxy, except for two small air holes; the sample is added via one while air escapes via the other. After adding the sample, the two openings are sealed with epoxy. The chamber's shape is described in Fig. 1: a very long chamber with a broad range of thicknesses. Due to the Mylar film, the glass surfaces are not parallel but very slightly angled at 0.4° relative to one another. Within our field of view, the change in our sample's thickness due to our sample chamber's slight taper is less than 0.3 μm, which is negligible for all but the thinnest regions. We do not see any influence of the taper in any of our results, suggesting it is reasonable to consider the two boundaries as locally quasiparallel. We define y as the direction along which the thickness H varies.

When we fill our slides with sample, a small fraction of particles stick to the sample chamber's walls. Typically less than 20% of the walls' area is coated with stuck particles [37]. The stuck particles are easy to identify as their apparent motion, due to noise inherent to particle tracking, is much less than the other particles. An image showing the locations of some stuck particles is shown in Fig. 2. Other observations confirm that both large and small particles stick to the walls [37]. We find that the particles stick to the surfaces of the glass slides only during the initial loading of the sample chamber with colloid. The stuck particles remain stuck indefinitely, through a van der Waals attraction to the glass, and are a permanent feature of the surface. The mobile particles do not stick to the sample's glass boundaries over time—during the experiments they never are seen to stick, and over several months the amount of particles stuck to the glass does not appear to change. In fact, the mobile particles are repelled from the glass boundaries by a relatively weak Coulombic interaction; in other words, during the course of the experiment, the only particle-wall interaction is a weakly repulsive one. In a sample of dilute colloids, we observe that the concentration of particles is low at the wall and approaches the bulk value quickly, within 0.5 ± 0.1 μm, suggesting that the Debye screening length is ≈0.4 μm at most and more likely

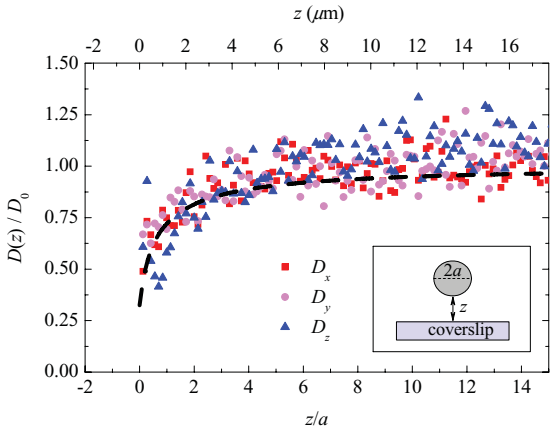

FIG. 3. (Color online) Measurements of local diffusion constants as a function of the distance z to the wall, normalized by the particle radius $a = 1.18\ \mu$m. The data are from a monodisperse dilute suspension. The dashed line is Faxen's Law [40,41]. (Inset) Sketch indicating that $z = 0$ corresponds to the particle touching the wall.

$\approx 0.2 - 0.3\ \mu$m, in agreement with prior observations [38]. The stuck particles are expected to slightly slow adjacent particles [39], which has been confirmed in our experimental data [37].

Particles do interact with the wall hydrodynamically. In the same dilute suspension, we measure particle mobility near the glass walls, with measured diffusivity shown in Fig. 3 as a function of the distance z from the wall. The behavior (symbols) is in good agreement with Faxen's Law (dashed line) [40,41] which quantifies the hydrodynamic influence of a planar boundary. Of course, the hydrodynamic behavior is modified in confinement approaching quasi-two-dimensional situations, where the sample chamber thickness H is comparable to the particle size $2a$ [42–44]. We do not consider experiments that are this thin; our observations all have $H \gtrsim 6a$. More significantly, for the larger volume fractions we consider in this work, the hydrodynamic interaction will be screened by the other particles, and so will not depend so strongly on the distance from the wall [44,45].

III. RESULTS

A. Wall-induced structure

We use the positions of the stuck particles to measure the local thickness of the sample chamber. To do this we find the number density $n(z)$ as a function of the distance z between the walls, shown in Fig. 4 for (a) the mobile particles and (b) the stuck particles. The maximum of each peak in Fig. 4(b) corresponds to the approximate position of the *centers* of the small particles stuck to the sample's walls. These positions are marked by the vertical dashed lines in Fig. 4, whose separation indicate the *effective* local chamber thickness H. Since only the small particles are visible to the microscope, the actual thickness is $H + 2a_{\text{small}} = H + 2.36\ \mu$m. The mean particle radii are known only to within $\pm 0.02\ \mu$m, while our uncertainty in their z positions is $0.1\ \mu$m. By averaging over tens of stuck particles we can determine H to within $0.01\ \mu$m.

Figure 4(a) shows layering of particles near the sample walls, which has been seen in both computer simulations

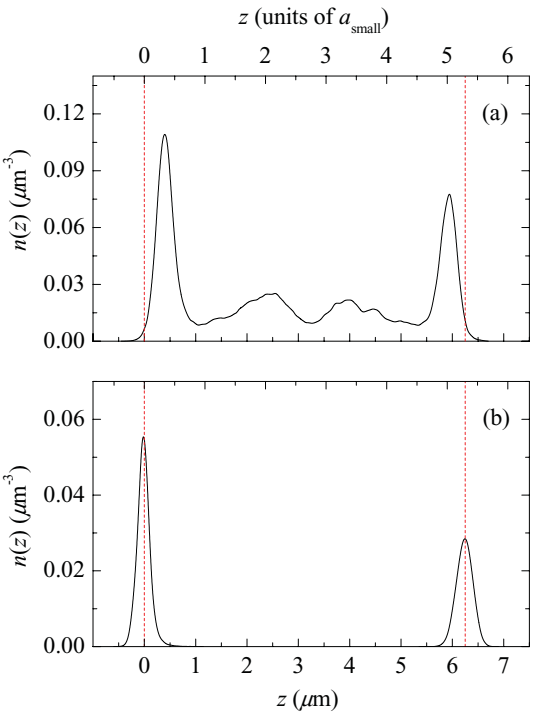

FIG. 4. (Color online) The number density n as a function of the distance z between the walls, for the visible (small) particles. (a) All mobile particles. (b) All immobile particles. The vertical lines in both indicate the position of the centers of the visible particles stuck to the walls. For this data, the distance between the two positions is $H = 6.25\ \mu$m, the effective local chamber thickness.

[6,46] and experiments [11,30,35,39]. Comparing Fig. 4(a) to Fig. 4(b) we see that the boundary layers of the mobile particles are offset from those of the stuck particles. The offset is due to Coulombic repulsion between the glass walls and PMMA particles, and is about $0.4\ \mu$m in all cases. Using differential interference contrast (DIC) microscopy, we confirm that the large particles also form layers, albeit in positions shifted due to their size. Our results are qualitatively in agreement with simulations that studied layering of binary mixtures of particles near walls [47,48], and are fairly similar to observations of layering in single-component colloidal samples [11,30,39].

Figure 5 displays the way layering changes with H. The peaks of $n(z)$ are tallest and thinnest next to the walls. Subsequent layers are shorter and wider, presumably as the correlations between particle positions become diluted through the presence of two particle sizes [47]. Note that we do not see any "quantization" effects for particular values of H [49]. For example, some packing effects were seen in simulations at $H = 2ma_{\text{small}} + 2na_{\text{large}}$ for integer values m,n, but these effects are too subtle to be resolved given the relatively few values of H for which we have experimental data [47].

B. Sample-averaged dynamics

Before we consider the specific influence of the particle layers on the particle motion, we will quantify the average motion of the sample. This is done by calculating the mean square displacement (MSD) as

$$\langle \Delta x^2 \rangle = \langle [x_i(t + \Delta t) - x_i(t)]^2 \rangle_{i,t},$$

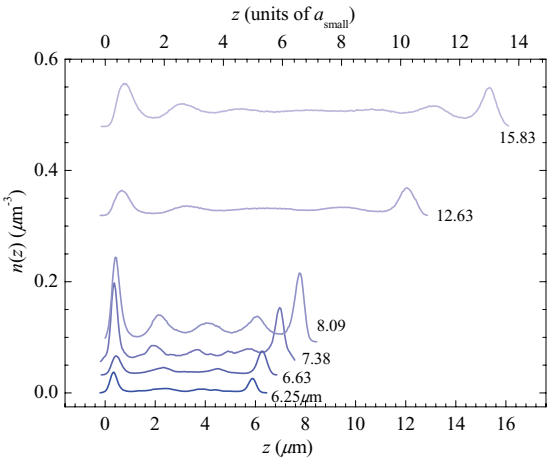

FIG. 5. (Color online) Number density n as a function of the distance z between the walls. The thickness H is as labeled (in microns). The values of H in terms of a_{small} are 5.30, 5.62, 6.83, 6.86, 10.7, and 13.4. The curves are vertically offset for clarity, where the offset is proportional to H. Where there is an asymmetry in the height of the $z \approx 0$ peak and the $z \approx H$ peak, it is due to one wall having more stuck particles on it, thus decreasing the room available for mobile particles.

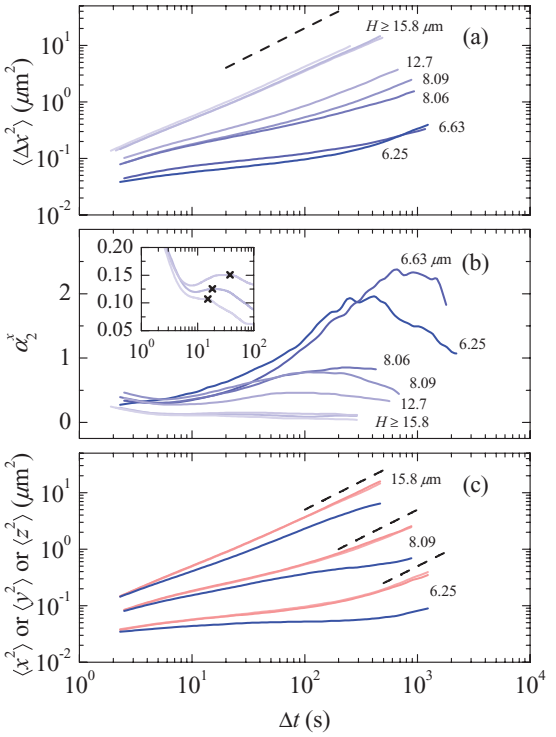

FIG. 6. (Color online) (a) The mean square displacement for our sample over a range of thicknesses [17]. The dashed line has a slope of 1.0. (b) Plots of the corresponding non-Gaussian parameter for each thickness. The x superscript of α_2^x is to indicate that the non-Gaussian parameter is only calculated using the x displacements (parallel to the wall, and perpendicular to the slight gradient in H). The inset is a magnification of the curves for $H \geqslant 15.8$ μm, with each curve's local maxima labeled, corresponding with Δt^* for the data at these thicknesses. (c) Components of the MSD curves. Light gray (red) curves are the x and y components of motion (parallel to the walls) and the dark gray (blue) are the z component of motion (perpendicular).

where the average is taken over all particles i and all initial times t. Analogous formulas apply for $\langle y^2 \rangle$ and $\langle z^2 \rangle$. Figure 6(a) shows that the motion parallel to the walls slows dramatically with confinement (decreasing H, as indicated). For values less than $H \approx 16\mu\text{m} \approx 14a_{\text{small}} \approx 10a_{\text{large}}$ we observe a systematic slowdown.

The change of shape of the curves in Fig. 6(a) suggest that confinement induces caging dynamics. This is the inhibited motion of a particle due to its "cage" of neighboring particles [50–54]. At the earliest times ($\Delta t < 1$ s, not shown), particle motion is diffusive as particles have not moved far enough to encounter the cage formed by the neighboring particles [55]. As the particle displacement becomes larger, its motion is impeded by its neighbors which form the cage, resulting in a greatly decreased slope of $\langle \Delta x^2 \rangle$ for $\Delta t < 100$ s. For smaller values of H, the decreasing height of $\langle \Delta x^2 \rangle$ in this range suggests that the cage size decreases in more confined samples. This is likely due to the concentration of particles into the layers (Fig. 5), which crowds them within the layers and reduces their cage sizes. Returning to Fig. 6(a), the upturn at larger Δt for $\langle \Delta x^2 \rangle$ is the result of cage rearrangements [7,22,51,53]. The neighbors rearrange and this lets the caged particle move to a new position. The motion of particles at longer lag times is diffusive due to the uncorrelated cage rearrangements [53]; this is not quite seen in our data sets here as the time scales for this diffusive motion is longer than our observation times. The results shown are for one volume fraction; our prior work showed that for larger ϕ, the onset thickness H for the confinement-induced slowdown increases [17].

To compare the mobility in the parallel and perpendicular directions, in Fig. 6(c) we plot $\langle \Delta x^2 \rangle$, $\langle \Delta y^2 \rangle$, and $\langle \Delta z^2 \rangle$ separately for several thicknesses. Not surprisingly, the mobility is less in the z direction (perpendicular to the wall). Furthermore, the upturn of the MSD at large Δt is barely beginning for the z data. The contrast between the parallel (x and y) and perpendicular (z) motion suggests that cage rearrangements may favor motions parallel to the walls.

The MSD curves show an overall slowing down due to confinement, but obscure the influence of the density layers on the motion. Figure 7(a) shows the number density for one data set. In panels (b) and (c) we plot the components of the MSD for fixed values of Δt. The dips in $\langle z^2 \rangle$ [Fig. 7(c)] coincide with the layers in Fig. 7(a) and imply that particles within layers are in a preferred structural configuration and are less likely to move elsewhere [6,11,17,46,49]. Meanwhile, the parallel component of motion shows no variation with z, even for long time scales. Our observations differ from one prior experiment by Eral *et al.* [11]. They found a decreased parallel mobility near the walls but did not measure perpendicular mobility. One difference is that they studied a single-component sample with a polydispersity of 8%, whereas we study a binary sample. Another difference is that their experiment had a spatial gradient in volume fraction due to nondensity matched particles (they have a density difference between solvent and particles of $\Delta\rho \approx 800$ kg/m^3, much larger than our value $\Delta\rho \approx 0.3$ kg/m^3).

Intriguingly, our results shown in Figs. 5, 7 and 8 look strikingly similar to recent experiments by Wonder, Lin, and Rice

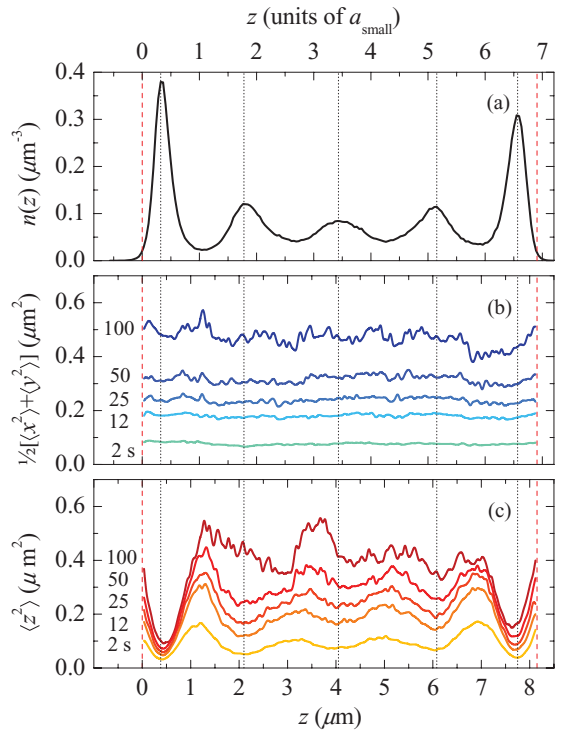

FIG. 7. (Color online) (a) Particle number density $n_{\text{small}}(z)$ as a function of distance z across the sample cell. Additional particles are permanently stuck to the walls of the cell (not shown) which have centers located at $z = 0.00$ μm and $z = H = 8.06$ μm, indicated by the vertical dashed lines. These data correspond to the $H = 8.06$ μm data in Fig. 6. (b) Mean square displacement parallel to the walls ($\frac{1}{2}[\langle \Delta x^2 \rangle + \langle \Delta y^2 \rangle]$) and (c) perpendicular to the walls ($\langle \Delta z^2 \rangle$) as a function of the particles' initial positions z. The displacements are calculated using a range of Δt, as labeled. The dotted lines indicate the position of the number density maximum of each layer in (a) while the dashed lines correspond to the approximate position of the centers of the particles stuck to the glass walls.

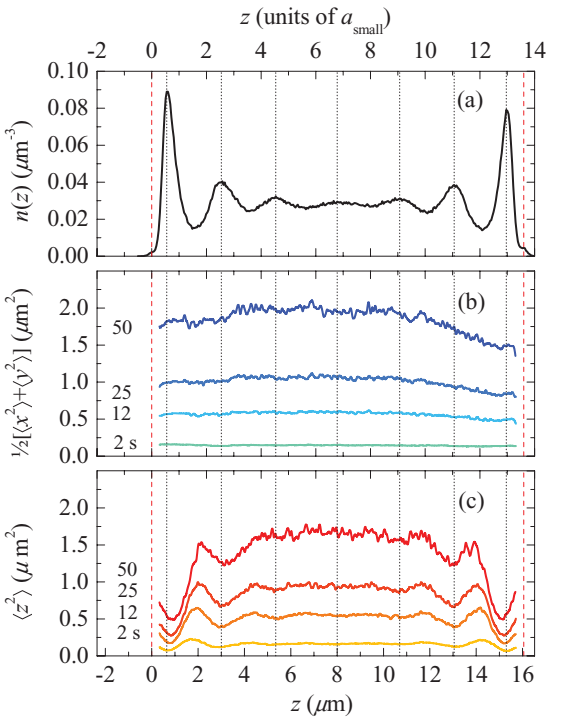

FIG. 8. (Color online) (a) Particle number-density $n_{\text{small}}(z)$ as a function of distance z across the sample cell. Additional particles are permanently stuck to the walls of the cell (not shown) which have centers located at $z = 0.00$ μm and $z = H = 16.0$ μm, indicated by the vertical dashed lines. These data correspond to the $H \geqslant 15.8$ μm data in Fig. 6. (b) Mean square displacement parallel to the walls ($\frac{1}{2}[\langle \Delta x^2 \rangle + \langle \Delta y^2 \rangle]$) and (c) perpendicular to the walls ($\langle \Delta z^2 \rangle$) as a function of the particles' initial positions z. The displacements are calculated using a range of Δt, as labeled. The dotted lines indicate the position of the number density maximum of each layer in (a) while the dashed lines correspond to the approximate position of the centers of the particles stuck to the glass walls.

[44]. They studied a monodisperse quasi-two-dimensional colloidal system, where particles were limited to one layer in z, and further constricted in y analogous to our confinement in z. They found that their experimental short-time diffusion coefficients had a similar qualitative behavior to what is shown in Figs. 7(b) and 7(c) [44]. They did not study long-time diffusion coefficients.

Our observed reduced particle mobility perpendicular to the walls is similar to the observations of Dullens and Kegel, who studied the first layer of colloidal particles at a smooth glass surface [30,31]. In their work, quasi-two-dimensional (q-2D) layers of particles formed along the surface of a glass slide in a bulk polydisperse colloidal suspension, just as we observe. Their wall-based particles only intermittently exchanged with the bulk particles [31]. In their q-2D wall layer, particles exhibited two-dimensional behavior that was fundamentally distinct from the dynamics of the particles further from the wall. However, a primary reason for this was that the particles were fairly monodisperse, and thus could form ordered 2D phases [30,31]. While we have pronounced layers near the walls for small H experiments, our samples are binary. DIC microscopy confirms that our two particle sizes remain well mixed in these layers and do not form ordered 2D phases. In addition, Figs. 7 and 8 show that slowing is not restricted to these layers alone. Note that the hydrodynamic interaction of particles with nearby walls diminishes as the volume fraction is increased [45].

One explanation for the slower dynamics might be that the volume fraction is larger in confinement. We first consider an observation from our experiment: The pair correlation function $g(r)$ changes slightly upon confinement, as shown in Fig. 9. This function indicates the likelihood of finding a particle a distance r away from a reference particle at $r = 0$, and so the first peak position indicates a typical spacing between nearest neighbor particles. For ideal hard spheres this first peak position is always at contact ($r_{\text{max}} = 2a_{\text{small}}$). Our particles are slightly charged, so the first peak shifts to larger values. The peak is additionally rounded by our finite resolution and the particle polydispersity [33]. Given the particle charges, an approximate expectation is that $\phi \sim r_{\text{max}}^{-3}$. The inset to Fig. 9 shows that confinement causes r_{max} to shift to lower values, which would correspond in an increase of ϕ from 0.42 to 0.49. One explanation for this is that, given the layering of particles, the local volume fraction within a layer is higher than 0.42, and $g(r)$ is reflecting this local volume fraction

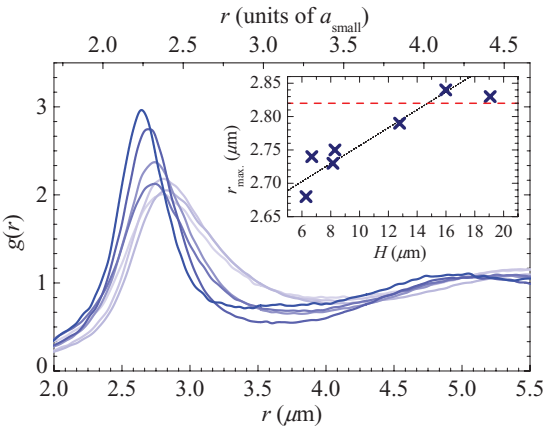

FIG. 9. (Color online) The pair correlation function $g(r)$ for a range of H. Darker curves correspond with thinner samples. The curves are from samples with thickness H equal to 6.25, 6.63, 8.09, 12.6, 15.8, and 18.9 μm, along with one curve for the sample's bulk (the lightest color curve). The inset shows the position of the first peak as a function of H. The red horizontal dashed line indicates $r_{\max}$ for the bulk sample, while the diagonal dotted black line is a guide to the eye.

[which would be more heavily weighted in the average used to calculate $g(r)$]. Another possible explanation is that the sample chamber is effectively thinner than we believe, due to the interactions between the particles and the walls. As noted above, the particle concentration is diminished within 0.4 μm of the walls. At the thinnest regions we study, $H \approx 6$ μm; if the true value is $\approx$5.2 μm, this would correspond to an increase of ϕ from 0.42 to $0.42 \times (6/5.2) \approx 0.48$, consistent with the estimate from the $g(r)$ data. However, an effective volume fraction increase from 0.42 to 0.49 seems unable to explain all of the dramatic slowing of the dynamics seen in Fig. 6(a). Consider the data at $\Delta t = 100$ s: $\langle \Delta x^2 \rangle$ drops by a factor of $\sim$40 going from the bulk to $H = 6.25$ μm. A study of an unconfined binary suspension similar to ours found a drop of $\sim$3.7 for a change of ϕ from 0.42 to 0.49 [33]. Thus we are left with a factor of 10 in additional slowing which is not due to a possible volume fraction change. This agrees with the conclusions of Eral *et al.* [11].

C. Defining cooperatively rearranging regions

The features of our $\langle \Delta x^2 \rangle$ curves resemble those of bulk supercooled colloidal liquids, where cage rearrangements play a significant role in the material's underlying dynamics. The process of cage rearrangements leads to a liquid's overall structural relaxation [56,57]. Adam and Gibbs were the first to hypothesize the existence of "cooperatively rearranging regions" (CRRs) as a supercooled liquid's means of increasing its configurational entropy [1]. Prior simulations [2,58,59] and experiments [21,22,60] found cooperatively moving regions, defined as groups of neighboring molecules or particles that collectively rearrange their positions. The connection between these observations and the CRRs of Adam and Gibbs is perhaps problematic [61]. Nonetheless, it is certainly intriguing that spatially heterogeneous dynamics have been seen in a wide range of glass-forming systems [3]. We wish to see how the character of spatially heterogeneous motions changes upon confinement.

The precise definition of a cooperatively rearranging region is open to interpretation. Our definition is described below, and comprises of three key elements: (1) the time scale used to determine displacements, (2) the threshold for considering a displacement to be a "rearrangement," and (3) the definition of which particles are adjacent, such that their motion is "cooperative."

We first define the time scale of interest. Prior work found that a good choice is based on the shape of the probability distribution of displacements. Rearranging particles have displacements which are larger than normal, and thus lie in the tails of the distribution [21,22,60,62,63]. The size of the distribution tails is quantified by the non-Gaussian parameter α_2,

$$\alpha_2(\Delta t) = \frac{\langle \Delta x^4 \rangle}{3\langle \Delta x^2 \rangle^2} - 1,$$

from Ref. [64]. The maximum of α_2 defines the cage rearrangement time scale Δt^*. We plot $\alpha_2(\Delta t)$ in Fig. 6(b): Both the maximum value of α_2 and the time scale Δt^* increase with decreasing H, similar to prior observations on a monodisperse sample [19]. For data from $H \geqslant 15.8$ μm, the levels of noise at low values of Δt manifest as a false increase of α_2, so we ignore this peak. For $\Delta t > 10$ s there are secondary local maxima of α_2 that we consider to be a better determinant of Δt^* [see the inset plot of Fig. 6(b)]. We plot Δt^* versus H in Fig. 10(a), which decays roughly exponentially with H until $H \approx 20$ μm, at which it reaches the bulk value. Simply put, as H decreases the displacement distributions become less Gaussian-like, and the time scale Δt^* for which the distributions are most extreme grows.

To define the length scale which separates a "rearranging" displacement from a "caged" displacement, we use a mobility threshold Δr^*. Both experiments [22,65] and simulations [66] have used a displacement threshold to define mobility such that over time, some percentage of the particles have displacements $|\Delta \vec{r}| \geqslant \Delta r^*$ [2,66], although at any given time the fraction may not be exactly this percentage. Thresholds of the top 5th percentile [22,66], 8th percentile [53], 10th percentile [65], and 20th percentile [67] have all been used to define Δr^*. From examining distributions of Δx and Δy for our data for each H, we find that the slowest 90% of the displacements are well described by a Gaussian distribution, whereas the top 10% are more probable than a Gaussian distribution would predict. Thus, we define our mobility threshold as the top 10% of the most mobile particles. Displacements in the z direction, however, vary significantly with H, making their inclusion in the calculation of our threshold impractical. As is the case with prior studies [2,22], our choice of Δr^* is somewhat arbitrary and our results are robust to some variation of Δr^*.

To complete our identification of CRRs we must identify which highly mobile particles are simultaneously nearest neighbors. Similar to other work, we define neighbors as those particles whose separation is less than a cutoff distance set by the first minimum of the pair correlation function $g(r)$ [53]. Our distributions of $g(r)$ do not vary substantially with H, as shown in Fig. 9. We use the average position of the first

minimum (3.87 μm) to define particles which are nearest neighbors.

One problem we face is the selective visibility of the colloidal particles. As discussed earlier, only the smaller particles of our binary suspension are fluorescent meaning that the larger species of particles are not visible to our confocal microscope. Despite this limitation we can still draw some reasonable conclusions. For example, in a study of a binary colloidal suspension similar to the one studied here, Lynch *et al.* showed that the cooperative dynamics of one species were similar to that of the other [67]. Mobile particles of one species were usually near mobile particles of the other species. Therefore, it is reasonable to draw some conclusions about cooperative motion from the small particles alone. One other related limitation is that small rearranging particles may not be nearest neighbors, but may be part of the same CRR, connected by unseen large particles. This may simply limit the apparent sizes of CRRs without otherwise changing their character.

D. Shapes of cooperatively rearranging regions

We first visualize these CRRs to develop a qualitative understanding of their nature. Figure 11 depicts clusters of mobile particles in a sample with $H = 15.8$ μm and 6.63 μm [Figs. 7(a) and 7(b), and Figs. 7(c) and 7(d), respectively). For clarity, bonds have been drawn between particles that are nearest neighbors (i.e., within a cluster). Groups of mobile particles can be seen for both thicknesses. The size of these mobile clusters in the unconfined sample is small, as expected for this low volume fraction ($\phi = 0.42$) [22]. Despite their small size, these mobile clusters are the primary means for particle rearrangements in the sample. The sample can be considered as composed of the slowest 90% particles which are caged at a given moment, and the rearranging fastest 10%. If the nature of the fastest 10% changes in confinement—for example, if those rearrangements occur less frequently—then the overall sample diffusivity will decrease.

Confinement induces slower dynamics, and in the bulk slower dynamics are associated with larger CRRs [21,22]. Perhaps confinement induces a similar larger size of CRRs [19]; but at first glance, comparing Figs. 11(a) and 11(c) might suggest that the cluster sizes are smaller upon confinement. However, recall that the particles shown are the most mobile 10%; the thinner sample has fewer particles in the imaged volume, and thus 10% of this smaller number results in fewer mobile particles to show without necessarily implying that the CRRs are smaller. To quantify the size of CRRs we calculate the mean number of particles in a CRR N_C as a function of H, plotted in Fig. 10(b). Figure 10(b) shows that CRRs involve roughly the same number of particles, regardless of thickness. The mean CRR size is between three and four particles, but this is only slightly larger than the minimum size of three particles. The small size may be because the bulk sample, with $\phi = 0.42$, is liquidlike and only has small CRRs [22]. Alternatively, as noted above, we cannot see the large particles which are almost certainly part of CRRs [67]. With the data of Fig. 10(b), we cannot say clearly if the CRRs are larger or smaller upon confinement. There is a very slight downward trend in $\langle N_C \rangle$ with decreasing H, but this could be due to poor

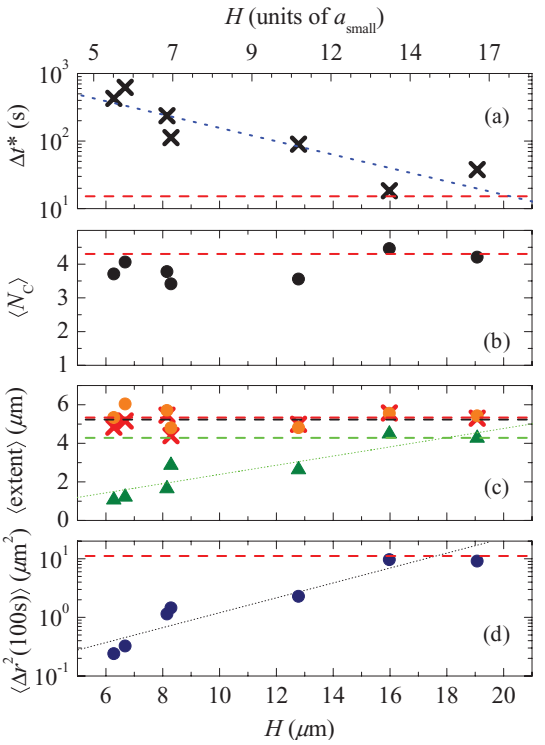

FIG. 10. (Color online) (a) Values of Δt^* that maximize α_2 for a range of thicknesses H. The horizontal dashed line indicates the value of Δt^* for the bulk sample. (b) Plot of the mean number of particles within cooperatively rearranging regions, as a function of H. Only $N_C \geqslant 3$ are considered to avoid trivial rearrangements that consist of one or two particles. The dashed line indicates $\langle N_C \rangle$ for the sample's bulk. (c) Plot of the average extent of cooperatively rearranging regions parallel (crosses and circles correspond to x and y, respectively) and perpendicular (triangles, z) to the sample's walls. The difference between the x and y data is an indication of the amount of uncertainty in our data. The upper and lower horizontal dashed lines indicate the mean horizontal and perpendicular extent of data from the sample's bulk, respectively. In principle these should be the same (the behavior should be isotropic in the bulk); in practice the lines may differ due to finite data or anisotropy in the imaging volume (50 μm in x and y but only 20 μm in z). (d) Value of the mean square displacement $\langle \Delta r^2 \rangle$ at the time scale $\Delta t = 100$ s. The horizontal dashed line indicates the value of the bulk sample. In panels (a), (c), and (d), the dotted lines are guides to the eye.

statistics. It is possible that the influence of confinement on the size of CRRs would be clearer in a sample with a larger value of ϕ, although such samples are very difficult to load into our thin sample chambers (as has been noted by others [68,69]). Likely some of the difficulty in loading the samples is due to their increasing glassiness in confined spaces. Results from another confocal microscopy experiment on a monodisperse sample suggested that the length scale for CRRs grows upon confinement [19]. The difference from our results may be due to our use of a binary sample.

An alternate way to quantify the size of a CRR is through its spatial extent. We define the spatial extent of the CRRs as $x_{\text{extent}} = \max(x_i) - \min(x_i)$, where i ranges over all particles within a given CRR. Similar definitions apply for the y and z directions. We plot the mean CRR extent in the x, y, and

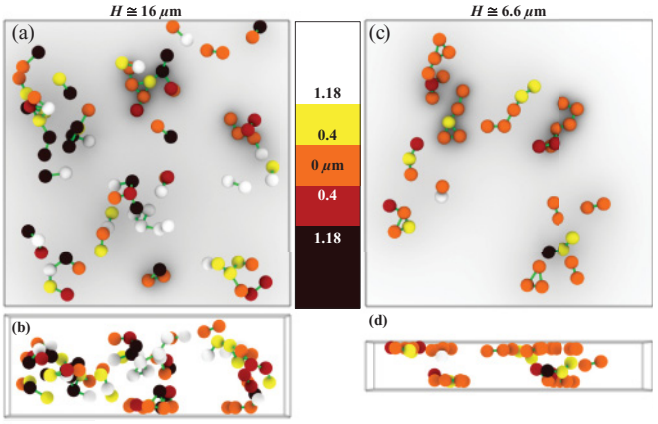

FIG. 11. (Color online) Three-dimensional renderings of the top 10% most mobile particles in two different sample thicknesses. The bonds between particles are drawn only to indicate nearest neighbors and do not imply physical connections. Only groups with $N_C \geqslant 2$ particles are drawn. The colors correspond to the magnitude of displacements in the z direction, normal to the confining boundaries. The experiment's field of view, and the effective position of the confining boundaries, are indicated by the light gray bounding boxes. The sample on the left [(a) and (b)] has a thickness of $H = 15.8$ μm and the one on the right [(c) and (d)] has $H = 6.63$ μm. The top row of images [(a) and (c)] view the sample normal to the confining boundaries, while the bottom row [(b) and (d)] provide a parallel view. Black and white indicate displacements of at least a_{small} over a $\Delta t = 23$ s and 250 s for the thicker and thinner sample, respectively.

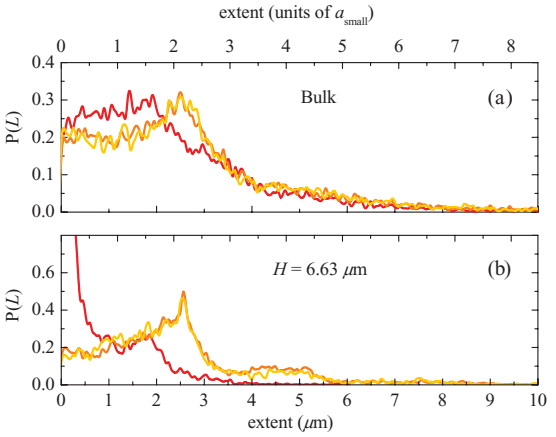

FIG. 12. (Color online) Extent of mobile groups of particles. Dark and light gray (red and orange online) indicate the perpendicular and parallel extents, respectively. CRRs in the bulk (a) of the sample are more isotropic in shape than when confined (b) to $H = 6.63$ μm. Note the difference in vertical scales used by the two plots. Only CRRs consisting of at least three particles are considered in the data shown.

z directions separately in Fig. 10(c). We find that the CRRs maintain a constant size in the direction parallel to the walls. However, the amount of distance that the CRRs extend in the direction perpendicular to the walls is significantly smaller than H, and decreases as H decreases. In the z direction, then, clusters are smaller, perhaps trivially because CRRs have to fit into a thinner sample chamber. Comparing this result with the $\langle N_c \rangle$ data of Fig. 10(b) suggests that the CRRs are becoming more compact in z with the same number of particles. This suggests that perhaps they are fractal in the bulk with a fractal dimension larger than 2 (as seen previously in Ref. [22]) and become more planar upon confinement (fractal dimension approaching 2).

The onset of flatter or more planar CRRs coincides with the sample's overall slowing. In Fig. 10(d) we plot the MSD values from Fig. 6(a) for $\Delta t = 100$ s against the corresponding range of H. We observe that the MSD values of Fig. 10(d) begin to deviate from those of the bulk, indicated by the horizontal dashed line in (d), at approximately the same H that the z extents of the CRRs first begin to flatten relative to the z extent from the bulk, the horizontal dashed line in Fig. 10(c). This is the strongest evidence linking the changing CRRs to the slowing dynamics. The overall concept is that confinement modifies the structure from that of the bulk, and this changed structure leads to slower dynamics [48].

To more carefully quantify the shapes of the CRRs, we consider the probability distributions of the extents in the three directions. These distributions are shown in Fig. 12 for a bulk sample (a) and a confined sample (b). In the unconfined sample the distributions for the x, y, and z directions are approximately the same, as should be expected; these CRRs are spatially isotropic. Differences in the z are most likely due to minor particle position errors which are larger in z, as discussed in Sec. II. Figure 12(b) looks quite different. The extent in z is nearly zero for a majority of CRRs [red (dark gray) curve in Fig. 12(b)]; these are planar CRRs and are overwhelmingly more probable than in the unconfined case. A small subset of confined CRRs do extend into the z direction by one to two particle diameters. The clusters of rearranging particles along the walls in Figs. 11(c) and 11(d) seem to be the most planar in shape. Thus we are led to conclude that the CRRs in the confined cases are qualitatively different than those of the unconfined sample.

E. Details of rearrangements

We next investigate the behavior of particles within CRRs. In Fig. 11 the particles are colored in correspondence with their amount of perpendicular motion, as shown in the key. In the confined situation mobile particles displace horizontally more frequently than otherwise, as suggested by the greater number of orange (medium gray) particles in Figs. 11(c) and 11(d), This makes sense: A rearrangement consisting of particles within a single layer does not require the particles to move vertically for the rearrangement to occur. Occasionally we do see particles which jump between layers or even swap between layers; one example is near the bottom right corner of Fig. 11(c).

To compare the amount of parallel versus perpendicular displacements, we calculate the directions of motion for all particles and then repeat the comparison for different confinement thicknesses. Using a spherical coordinate system we determine the polar angle of a given particle displacement. The polar angle θ spans a range from 0° to 180°, which corresponds to motion toward or away from the nearest sample chamber wall, respectively. That is, we exploit the symmetry

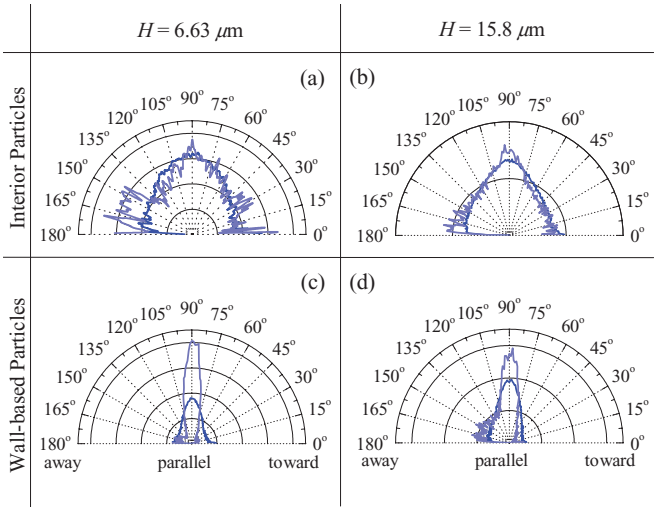

FIG. 13. (Color online) Polar plots of the probability distributions of the directions of particle displacements for $H = 6.63$ and $H = 15.8$ μm as indicated. (a) and (b) Data for the two thicknesses, considering only particles away from the walls. (c) and (d) Data for particles in the layers immediately adjacent to a wall. The displacements from one wall are reversed, so that 180° always means motion away from the nearest wall. In all panels, the light blue curve (light gray) is the distribution for the most mobile 10% of the particles, while the dark blue curve (dark gray) is the distribution for all particles. Displacements are measured over $\Delta t = 250$ s and $\Delta t = 23$ s for the $H = 6.63$ μm and $H = 15.8$ μm data, respectively.

between the two walls. We first compute the polar angle θ relative to the $+z$ axis, and then use $180^\circ - \theta$ for the data in the lower half of the sample chamber. Comparing the data separately for the top and bottom half, we find no difference in the results. For isotropic motion, the distribution of θ is proportional to $\sin\theta$, so we divide our measured histograms by $\sin\theta$ to remove this dependence. The distributions are plotted in polar coordinates, shown in Fig. 13, for thicknesses of $H = 6.63$ μm and $H = 15.8$ μm. The dark curves are for all particles, and the light curves are for the top 10th percentile of displacements, providing insight into the directions that tend to permit higher mobility. The top panels show the motion of the particles in the interior of the sample, and the bottom panels show the motion of the particles immediately adjacent to the walls.

In both the 15.8-μm and 6.63-μm samples, the particles in the outer layers along the walls tend to move parallel to them ($\theta \approx 90^\circ$) rather than perpendicularly [Figs. 13(c) and 13(d)]. The effect is even more pronounced for the fastest particles, whose distribution suggests that fast particles move almost exclusively along the walls. This agrees with our observations from Figs. 11(b) and 11(d), where the particles layered along the walls are almost all orange (medium gray), indicating they are moving primarily horizontally. The distributions in Figs. 13(c) and 13(d) do show some data at $\theta = 180^\circ$, indicating that some particles move away from the walls, and less data at $\theta = 0^\circ$, indicating that some particles make slight motions toward the walls.

The situation changes markedly for the inner layers [Figs. 13(a) and 13(b)]. Considering only the full distribution of all particles we see that the displacements are more isotropic, although there is still a slight bias in the $\theta \approx 90^\circ$ direction. The distribution of directions for the most mobile interior particles is similar. There are bumps in these distributions near $\theta = 0^\circ$ and 180°, suggesting that particles that move in z have a slight increased probability to make large motions in z, hopping between layers.

Overall, the particle dynamics in the thicker region are far more isotropic than the ones from the confined region [compare Figs. 13(a) and 13(c) with 13(b) and 13(d)]. In the $H = 15.8$ μm case, there are appreciable signs of anisotropic behavior only along the walls.

IV. CONCLUSION

The smooth quasiparallel walls confining our sample induce the formation of density layers within the colloidal sample's volume. The most dense layers form along the sample chamber's glass surfaces, as shown in Fig. 5 and also observed in other experimental work that used single-component colloidal samples [11,30]. The structural inhomogeneities induced by the density layers result in corresponding inhomogeneities in the system's dynamics, as described by the plots in Figs. 7 and 8. Particles move most easily within their layer, but this is still slower than they would move in unconfined samples. The layered particles cooperatively rearrange within the layer but rarely with adjacent layers; the cooperative rearrangements occur in more planar-shaped groups of particles. Given that even in unconfined samples, particles need to move cooperatively if they wish to have large displacements, the change in the character of the cooperatively rearranging regions seems to explain the slowing dynamics. In short, the thickness at which we begin to observe the slowing in the sample's average dynamics corresponds with the confinement length scale at which cooperatively rearranging regions begin to become planar in shape [Figs. 10(c) and 10(d)]. Our prior work suggests that the observed increase in rearrangement time scales and the thickness at which these regions begin to flatten will both grow with higher volume fractions [17].

It is likely if the walls were roughened, the results might change. Simulations [6,7,10] and experiments [11,39] showed that behavior is often glassier with rough walls. With rough walls, layering is greatly diminished or prevented entirely, or perhaps becomes more subtle. For example, particles might form a corrugated layer wrapping around the local wall texture. This could then lead to other shapes for the cooperatively rearranging regions, the main point being that structure that departs from the bulk results in slower dynamics [48].

ACKNOWLEDGMENTS

We thank M. H. G. Duits, H. B. Eral, G. L. Hunter, and C. B. Roth for helpful discussions. Funding for this work was provided by the National Science Foundation (Grant No. DMR-0804174).

[1] G. Adam and J. H. Gibbs, J. Chem. Phys. **43**, 139 (1965).
[2] W. Kob, C. Donati, S. J. Plimpton, P. H. Poole, and S. C. Glotzer, Phys. Rev. Lett. **79**, 2827 (1997).
[3] M. D. Ediger, Annu. Rev. Phys. Chem. **51**, 99 (2000).
[4] M. Alcoutlabi and G. B. McKenna, J. Phys.: Condens. Matter **17**, R461 (2005).
[5] C. B. Roth and J. R. Dutcher, J. Electroanal. Chem. **584**, 13 (2005).
[6] Z. T. Németh and H. Löwen, Phys. Rev. E **59**, 6824 (1999).
[7] P. Scheidler, W. Kob, and K. Binder, Europhys. Lett. **59**, 701 (2002).
[8] K. L. Ngai, Philos. Mag. B **82**, 291 (2002).
[9] J. S. Sharp and J. A. Forrest, Phys. Rev. Lett. **91**, 235701 (2003).
[10] G. Goel, W. P. Krekelberg, J. R. Errington, and T. M. Truskett, Phys. Rev. Lett. **100**, 106001 (2008).
[11] H. B. Eral, D. van den Ende, F. Mugele, and M. H. G. Duits, Phys. Rev. E **80**, 061403 (2009).
[12] S. A. Rice, Chem. Phys. Lett. **479**, 1 (2009).
[13] C. B. Roth, K. L. McNerny, W. F. Jager, and J. M. Torkelson, Macromolecules **40**, 2568 (2007).
[14] Z. T. Németh and H. Löwen, Phys. Rev. E **59**, 6824 (1999).
[15] P. N. Pusey and W. van Megen, Nature (London) **320**, 340 (1986).
[16] A. van Blaaderen and P. Wiltzius, Science **270**, 1177 (1995).
[17] C. R. Nugent, K. V. Edmond, H. N. Patel, and E. R. Weeks, Phys. Rev. Lett. **99**, 025702 (2007).
[18] P. S. Sarangapani and Y. Zhu, Phys. Rev. E **77**, 010501 (2008).
[19] P. S. Sarangapani, A. B. Schofield, and Y. Zhu, Phys. Rev. E **83**, 030502 (2011).
[20] A. van Blaaderen, A. Imhof, W. Hage, and A. Vrij, Langmuir **8**, 1514 (1992).
[21] W. K. Kegel and A. van Blaaderen, Science **287**, 290 (2000).
[22] E. R. Weeks, J. C. Crocker, A. C. Levitt, A. Schofield, and D. A. Weitz, Science **287**, 627 (2000).
[23] A. D. Dinsmore, E. R. Weeks, V. Prasad, A. C. Levitt, and D. A. Weitz, App. Optics **40**, 4152 (2001).
[24] E. R. Weeks, J. C. Crocker, and D. A. Weitz, J. Phys.: Condens. Matter **19**, 205131 (2007).
[25] S. Granick, Phys. Today **52**, 26 (1999).
[26] P. A. Thompson, G. S. Grest, and M. O. Robbins, Phys. Rev. Lett. **68**, 3448 (1992).
[27] J. Goyon, A. Colin, G. Ovarlez, A. Ajdari, and L. Bocquet, Nature (London) **454**, 84 (2008).
[28] H. X. Zhou, G. Rivas, and A. P. Minton, Ann. Rev. Biophys. **37**, 375 (2008).
[29] D. G. Grier and C. A. Murray, J. Chem. Phys. **100**, 9088 (1994).
[30] R. P. A. Dullens and W. K. Kegel, Phys. Rev. Lett. **92**, 195702 (2004).
[31] R. P. A. Dullens and W. K. Kegel, Phys. Rev. E **71**, 011405 (2005).
[32] W. C. K. Poon, E. R. Weeks, and C. P. Royall, Soft Matter **8**, 21 (2012).
[33] T. Narumi, S. V. Franklin, K. W. Desmond, M. Tokuyama, and E. R. Weeks, Soft Matter **7**, 1472 (2011).
[34] J. C. Crocker and D. G. Grier, J. Colloid Interface Sci. **179**, 298 (1996).
[35] C. Murray, MRS Bull. **23**, 33 (1998).
[36] A. B. Fontecha, H. J. Schöpe, H. König, T. Palberg, R. Messina, and H. Löwen, J. Phys.: Condens. Matter **17**, S2779 (2005).
[37] K. V. Edmond, C. R. Nugent, and E. R. Weeks, Euro. Phys. J. - Spec. Top. **189**, 83 (2010).
[38] C. P. Royall, R. van Roij, and A. van Blaaderen, J. Phys.: Condens. Matter **17**, 2315 (2005).
[39] H. B. Eral, F. Mugele, and M. H. G. Duits, Langmuir **27**, 12297 (2011).
[40] H. Faxén, Ann. Phys. **373**, 89 (1922).
[41] K. Svoboda and S. M. Block, Annu. Rev. Biophys. Biomol. Struct. **23**, 247 (1994).
[42] J. Santana-Solano, A. Ramírez-Saito, and J. L. Arauz-Lara, Phys. Rev. Lett. **95**, 198301 (2005).
[43] D. T. Valley, S. A. Rice, B. Cui, H. M. Ho, H. Diamant, and B. Lin, J. Chem. Phys. **126**, 134908 (2007).
[44] E. Wonder, B. Lin, and S. A. Rice, Phys. Rev. E **84**, 041403 (2011).
[45] V. N. Michailidou, G. Petekidis, J. W. Swan, and J. F. Brady, Phys. Rev. Lett. **102**, 068302 (2009).
[46] A. J. Archer, P. Hopkins, and M. Schmidt, Phys. Rev. E **75**, 040501 (2007).
[47] K. W. Desmond and E. R. Weeks, Phys. Rev. E **80**, 051305 (2009).
[48] J. Mittal, V. K. Shen, J. R. Errington, and T. M. Truskett, J. Chem. Phys. **127**, 154513 (2007).
[49] J. Mittal, T. M. Truskett, J. R. Errington, and G. Hummer, Phys. Rev. Lett. **100**, 145901 (2008).
[50] E. Rabani, D. J. Gezelter, and B. J. Berne, J. Chem. Phys. **107**, 6867 (1997).
[51] A. Kasper, E. Bartsch, and H. Sillescu, Langmuir **14**, 5004 (1998).
[52] B. Doliwa and A. Heuer, Phys. Rev. Lett. **80**, 4915 (1998).
[53] E. R. Weeks and D. A. Weitz, Phys. Rev. Lett. **89**, 095704 (2002).
[54] P. M. Reis, R. A. Ingale, and M. D. Shattuck, Phys. Rev. Lett. **98**, 188301 (2007).
[55] M. Tokuyama, Physica A **378**, 157 (2007).
[56] M. D. Ediger, C. A. Angell, and S. R. Nagel, J. Phys. Chem. **100**, 13200 (1996).
[57] C. A. Angell, J. Phys.: Condens. Matter **12**, 6463 (2000).
[58] G. A. Appignanesi, J. A. RodriguezFris, R. A. Montani, and W. Kob, Phys. Rev. Lett. **96**, 057801 (2006).
[59] A. S. Keyes, L. O. Hedges, J. P. Garrahan, S. C. Glotzer, and D. Chandler, Phys. Rev. X **1**, 021013 (2011).
[60] A. H. Marcus, J. Schofield, and S. A. Rice, Phys. Rev. E **60**, 5725 (1999).
[61] C. Dalle-Ferrier, C. Thibierge, C. Alba-Simionesco, L. Berthier, G. Biroli, J. P. Bouchaud, F. Ladieu, D. L'Hôte, and G. Tarjus, Phys. Rev. E **76**, 041510 (2007).
[62] W. Kob, C. Donati, S. J. Plimpton, P. H. Poole, and S. C. Glotzer, Phys. Rev. Lett. **79**, 2827 (1997).
[63] C. Donati, J. F. Douglas, W. Kob, S. J. Plimpton, P. H. Poole, and S. C. Glotzer, Phys. Rev. Lett. **80**, 2338 (1998).
[64] A. Rahman, Phys. Rev. **136**, A405 (1964).
[65] A. S. Keys, A. R. Abate, S. C. Glotzer, and D. J. Durian, Nature Physics **3**, 260 (2007).
[66] C. Donati, S. C. Glotzer, P. H. Poole, W. Kob, and S. J. Plimpton, Phys. Rev. E **60**, 3107 (1999).
[67] J. M. Lynch, G. C. Cianci, and E. R. Weeks, Phys. Rev. E **78**, 031410 (2008).
[68] M. D. Haw, Phys. Rev. Lett. **92**, 185506 (2004).
[69] L. Isa, R. Besseling, A. N. Morozov, and W. C. K. Poon, Phys. Rev. Lett. **102**, 058302 (2009).